Chapter 3

Materials, Methods and Concepts

3.1 Experimental setup

3.1.1 The electrochemical cell

The detailed design of an electrochemical cell used for voltammetric studies strongly depends on the technique employed and the requirements of the chemical system being studied.

A very flexible cell design used for the single-crystal experiments in chapter 4 is shown in Fig. 3-1. Three separate compartments accommodate the working (WE), counter (CE) and reference (RE) electrode, respectively. The counter (g) and the working electrode compartment (a) were separated by a sintered glass (f) to prevent contamination of the main chamber. The reference electrode was placed in a Luggin-Haber capillary (c) which terminated a few millimeters away from the working electrode (b) in order to minimize the uncompensated ohmic drop across the electrolyte. After ionic connection through a thin liquid film had been assured, the stop cock of the reference electrode was kept in the closed position in order to minimize the leakage of the reference compartment. The teflon cap covering the main (working electrode) chamber is provided with several ports for the electrode holder and a gas-purging tube. The end of the purging tube was also fabricated by sintered glass in order to disperse the gas stream into fine bubbles. On the bottom of the main compartment a magnetic stirring (h) was placed to provide moderate laminar convective flows in front of the working electrode. During the experiments described in chapter 4, a Pt single crystal dipped into the electrolyte served as working electrode: After the crystal had been in contact with the electrolyte surface, it was slightly pulled up again to avoid electrode edge effects [88].

For the experiments reported in chapter 6, a cylindrical glass vessel of approximately 65 mm in inner diameter and 100 mm in height with gas inlets near the bottom was used as electrochemical cell. The inlets allowed the purging of the electrolyte prior to experiments. The gas outlets and all electrode connections were mounted into the teflon cap of the cell which also accommodated the capillary tubes serving as local

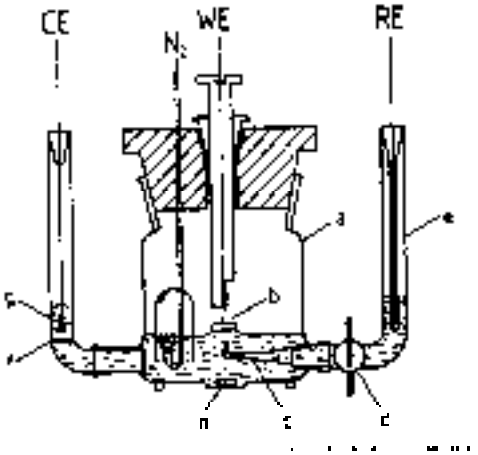

Figure 3-1: Conventional three- compartment three-electrode cell design as used for experiments of chapter 4. The working electrode is a single crystal dipped into the electrolyte.

potential probes (see geometrical details in section 3.2.3 or chapter 6). An additional gas inlet in the teflon cap provided an inert-gas atmosphere during experiments. In chapter 7 and 8, a conventional three electrode setup was used which hosted a working wire electrode (chapter 8) or a rotating-ring-disc electrode (chapter 7). The reference electrode compartment was again connected via a Luggin-Haber capillary in order to reduce the ohmic solution resistance. The counter electrode compartment was asymmetrically located outside the working electrode compartment connected by a sintered glass frit in order to avoid the diffusion of undesirable chemical species towards the working electrode. The solution resistance remains unaffected by the frit.

3.1.2 The Potentiostat/Galvanostat

Beginning in the 1950's most electrochemical experiments have been done with three electrodes and instrumentation built around a potentiostat. A common design based on an operational amplifier [89] is shown in Fig. 3-2. A true reference electrode is used to measure the potential; a voltage follower is attached to the reference electrode so that very little current is drawn in this part of the circuit. A counter (auxiliary) electrode is used to pass the bulk current. The positive input is at 0 V(ground) and the working (indicator) electrode is also at ground potential.

The current is measured by means of another operational amplifier circuit attached to the indicator electrode lead. Since the input resistance is high, all current must flow through the resistance R_2. However, the high gain of the amplifier produces an output voltage such that the potential at the inverting input is 0V. Thus, the working electrode is held at 0V as well, and the output potential is $-IR_2$, i.e. is proportional to the cell current.

Figure 3-2: Potentiostatcircuit for control of working electrode (=indicator electrode) potential in a three-electrode cell. Cell current is monitored with a current-follower circuit, and the reference electrode is protected from excessive current flow by an electrometer.

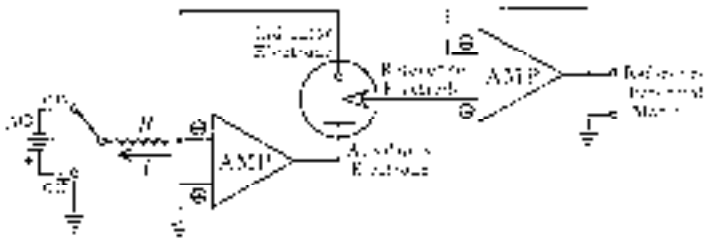

Figure 3-3: Galvanostat circuit for control of current through the cell.

Note that for control purposes (see chapter 7) the outer potential U is modified by the feedback loop signal through one of the potential control inputs. This means that the former constant parameter U turns into a time dependent variable.

The potentiostat mostly used in this work was provided by the electronic technical lab of the Fritz-Haber-Institute. The circuit is based on the idea of D. Roe [89]. For the ring-disc measurements (chapter 7) an EG&G bi-potentiostat/galvanostat served as power source.

In some experiments, a constant current is passed through the cell, and the potential of the working electrode is monitored using a reference electrode. An operational amplifier circuit which performs this function (a galvanostat) is shown in Fig. 3-3. Since the operational amplifier input resistance is high, the cell current must flow through resistor R. Feedback through the cell ensures that the working electrode stays at ground potential. Thus the potential drop across the resistor is equal to the battery potential and the cell current is $I = \Delta\Phi/R$.

3.1.3 Electrolyte solutions

All solutions were prepared using triply distilled water. Prior to experiments, solutions were purged with nitrogen (Linde technische Gase) in order to remove dissolved oxygen. In many experiments, the cell was kept under a nitrogen atmosphere during experiments to avoid oxygen diffusion into the solution. Details on chemicals, purities and concentrations of the electrolytes used in experiments can be found in the respective experimental sections of the forthcoming chapters.

3.1.4 Electrodes

Working electrodes

Single-crystal Pt electrodes. In chapter 4 low-index Pt single crystals were employed as working electrodes (WEs). The orientations used included Pt(100), Pt(110) and Pt(111) with an area of 0.6 cm^2 each. Most single crystals, purchased from Lamprecht Corp. (now MaTecK), were received in a cut, oriented and electropolished state. Otherwise the crystals were cut from a Pt rod (5N) in (100), (110) respectively (111) orientation. The precise orientation was determined by a Laue method ($\leq 0.5\ ^\circ$). The crystals were mechanically polished, followed by an electrochemical polishing at U=10 V. A Pt wire at the back of the single crystals served as electrical connection. This Pt wire was finally mounted into a teflon holder and contacted to the outer circuit (see Fig. 3-1).

Single crystals require a pretreatment before each experiment, as surface roughening occurs during electrochemical experiments. Also in the case of formic acid oxidation, organic impurities may deposit on the surface affecting the catalytic properties. Furthermore, surface atoms may considerably change sites after anodic OH ad- and desorption. In order to restore a (possibly roughned) single crystal surface to its pure orientation, flame annealing has proven to be the method of choice [90]. After the treatment of the single crystals at 1500 K, where ideally both organic compounds and surface roughness are removed, the crystal is carefully cooled down to room temperature either in water or in nitrogen. The quality of the resulting surface can be assessed by its cyclic voltammetric profile, in particular within the potential range of the ad- and desorption of hydrogen (-0.2 - +0.5 V vs Saturated Calomel Electrode, SCE), since the peak potentials of a clean surface are well known. Additional peaks or deviations in peak potentials indicate impurities.

Polycrystalline Pt (Pt-poly) electrodes . In chapter 4 and 7 polycrystalline Pt electrodes were employed in a rotating-disc arrangement. In chapter 6, a stationary Pt-poly ring electrode was pressed from a thin Pt plate. Polycrystalline electrodes require only relatively simple mechanical and chemical pretreatment. The electrode were first polished using Diaplast diamond paste (3 μm,1 μm,0.3 μm). Subsequent rinsing with ethanol and triply distilled water was to remove the paste remains. Thereafter, cyclic voltammetry between the hydrogen and oxygen evolution potentials was used to evaluate the cleanness of the electrode. In the case of the Pt plate ring electrode (chapter 6) a mixture of conc. sulphuric acid (suprapure) and hydrogenperoxide (30 %) was used as chemical pretreatment which was applied for about 10 to 120 min-

utes prior to experiments. The H_2O_2 solution was catalytically decomposed by Pt into molecular oxygen which destroyed all organic impurities. Subsequent rinsing in triply distilled water removed the remains of the acid. For details of the experimental procedures the reader is referred to the respective chapters.

Ag-poly electrode. In the experiments of chapter 8, a polycrystalline Ag wire and rotating Ag disc electrode were employed. The Ag electrodes were mechanically polished with Diaplast diamond paste (7 μm for wire, 1 -0.25 μm for disc). No cyclic voltammetry preceded the experimental investigations.

Counter electrodes

All counter electrodes were made from polycrystalline Pt wires. Their surface area should ideally exceed that of the working electrode. The geometries of the counter eletrodes used with respect to the WE included asymmetric arrangment as well as rotational symmetric arrangment in the case of a ring WE electrode.

Reference electrodes

In all experiments, a Hg/Hg_2SO_4 reference electrode was employed; its use proved to be convenient, since most systems studied throughout this thesis were operated in acidic solvents containing high sulphate ions. Thus, leakage problems or ionic impurities stemming from the reference compartment were negligible. Whenever potentials are reported throughout this thesis, however, the respective reference system will be indicated. Potentials referring to the Saturated Calomel Electrode are labelled with SCE.

3.1.5 Data acquisition

In chapter 7 and 8, current and potential data was read into a personal computer during electrochemical measurements in order to have the data available in digitized form and, as described in chapter 8 to calculate on-line a control signal which was then fed back onto the electrochemical system. The PC used was a Dell Dimension XPS P90 which collected external data via a GPIB- card PC II-A (General Purpose Interface Bus, IEEE 488) manufactured by National Instruments. Labview 4.0 was employed as software platform of the data collection and data output routines. The acquisition frequency was variable between 10 to 255 Hz.

3.2 Experimental methods

3.2.1 Cyclic Voltammetry

This method, where individual linear or triangular potential sweeps are applied to the working electrode, yields valuable information on the I/U characteristics of the electrochemical system considered. Both qualitative and quantitative information on thermodynamics and kinetics of the electrochemical processes can be drawn from the voltammetric profiles. Usually, in cyclic voltammetry one studies the I/U profile after

a number of cycles, when a steady voltammogram was obtained. A certain disadvantage of this popular methods is the fact that the electrochemical processes occurring at a given potential can depend on those that occurred at preceding potentials, i.e. on the history of the system. The latter phenomenon may not be confused with hysteresis. Important parameters of cyclic voltammetric methods include the initial and the reverse potential as well as the potential sweep rate. Processes accompanying charge transfer at solid electrodes such as ad- and desorption processes are conveniently recognized using cyclic voltammetric methods by their mirror-imaged peak potentials and their characteristic dependence of the peak current on the sweep rate.

3.2.2 The Rotating Disc and the Rotating Ring-Disc Electrode

The rotating disc electrode (RDE) is one of the most popular electrode types employed for the study of electrochemical processes. The RDE is consists of a metal electrode disc imbedded in a rod of insulating material. Here, mostly Pt and Ag disc electrodes will be used. Frequently, the imbedding material is teflon.

The major advantage of the RDE lies in the controllability of the convective conditions near the electrode surface. Mass transport which can complicate the I/U characteristics considerably can thereby be controlled at will; furthermore, the rotation frequency of the disc introduces an additional system parameter (constraint) characterizing the system.

Fig. 3-4 shows the hydrodynamic flow near the RDE. It is seen that as the RDE rotates, adjacent solution is pulled along by viscous drag and is pushed away from the axis of rotation by centrifugal force. The expelled solution is replaced by the flow normal to the electrode surface. Interestingly, these convective conditions can be solved analytically yielding important relations between the diffusion layer thickness, the concentrations and their gradient at the surface and the rotational frequency. Concentration profiles at an RDE can also be computed numerically. The concentrations gradients of the electroactive species are usually quite linear over some distance into the bulk solution which justified the Nernst diffusion layer approximation often employed in electrochemical modeling (see later chapters).

The hydrodynamics of the RDE can be exploited for obtaining mechanistic information by adding another electrode as a ring surrounding the disc electrode as shown in Fig. 3-5. This setup is referred to as the rotating ring-disc electrode (RRDE). Solution which flows to the central disc electrode is then flung outward by centrifugal force and flows past the concentric ring electrode. Thus, the solution arriving at the ring can be sampled and probed by electrochemical processes at the ring electrode. This allows measurements of the composition of the solution immediately at the disc and indirectly conclusions regarding the processes occurring on the disc itself. The key parameter is the collection efficiency N, i.e. the fraction of disc electrode product which can be sampled at the ring. The value of N only depends on the geometry (r1, r2, r3) and is independent of the rotational frequency. N can be calculated by using a rather messy equation (see [48], p. 302). For example, for an RRDE with r1=0.187 cm, r2=0.200 cm, and r3=0.332 cm, N =0.555, that is, 55.5 % of the product generated at the disc is collected at the ring. RRDE measuremnets can be most readily

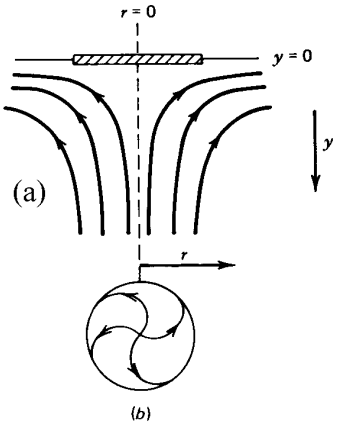

Figure 3-4: Schematic streamlines (convective flow) in laboratory frame at a rotating disc electrode (RDE). a) side view, b) top view.

interpreted in the diffusion-limited range since in this case the ring current can be quantitatively related to processes occurring at the disc, as consumption or production processes at the disc lead to detectable concentrations changes at the ring. Since two electrode potential must be controlled independently, a bi-potentiostat must be used.

The RRDE technique is commonly used either to arrive at qualitative conclusions as to intermediates occurring during electrochemical processes or to determine coverages or, especially in the field of chemical kinetics, to get insight into the phase behavior between the disc current and the concentrations of volume species near the disc [29]. The latter is of particular interest in oscillatory reactions because the phase relationship of oscillatory quantities provides valuable information in elucidating mechanisms.

3.2.3 Impedance spectroscopy

Impedance spectroscopy is a periodic potential perturbation technique in the linear regime applied to electrode processes in the steady state. In general impedance measurements determine the dependence of the total cell impedance on the perturbation frequency from which one can draw valuable kinetic information such as kinetic constants, bifurcation points and mechanistic information. The steady state considered must be stable against the perturbation applied to the measured system during the impedance measurements, otherwise the electrode process will not relax back to the original steady-state after the perturbation.

Figure 3-5: Schematic drawing of a rotating ring-disc electrode (RRDE)

Definition and calculation of impedance

Consider the case of a single potential-dependent chemical state variable θ [91], e.g. the relative surface coverage of an electrochemical species which ad- and desorbed and reacts electrochemically at the interface. Mass transport is to be neglected in the following treatment. The total faradaic current in the steady state I_{far} is a function of the double layer potential ϕ and θ :

$$I_{far} = f(\theta, \phi) \tag{3.1}$$

Upon small perturbations this expression can be expressed as a Taylor series yielding

$$\Delta I_{far} = \left(\frac{\partial I_{far}}{\partial \phi}\right)_{ss} \Delta\phi + \left(\frac{\partial I_{far}}{\partial \theta}\right)_{ss} \Delta\theta = \frac{\Delta\phi}{R_{ct}} + m\,\Delta\theta \tag{3.2}$$

where R_{ct} denotes the charge-transfer resistance of the electrode, i.e. the resistance when the influence of mass transport is neglected. The value of m may be positive or negative depending on whether the faradaic current is consuming θ or another nonessential adsorbed species. Thus, the faradaic admittance follows as

$$Y_{far} = \frac{1}{R_{ct}} + m\frac{\Delta\theta}{\Delta\phi}. \tag{3.3}$$

In order to calculate $\frac{\Delta\theta}{\Delta\phi}$, one has to consider the transient response of θ governed

by the dynamical evolution equation

$$\dot{\theta} = g(\theta, \phi) \tag{3.4}$$

where g represents the ad- and desorption as well as reaction terms affecting the concentration of θ. In the linear regime one can again write for the evolution of the perturbation $\Delta\theta$

$$\frac{d\Delta\theta}{dt} = \left(\frac{\partial\dot{\theta}}{\partial\phi}\right)_{ss} \Delta\phi + \left(\frac{\partial\dot{\theta}}{\partial\theta}\right)_{ss} \Delta\theta = g_\phi \, \Delta\phi + g_\theta \, \Delta\theta \tag{3.5}$$

where it is assumed that the steady state is stable, i.e. $\left(\frac{\partial\dot{\theta}}{\partial\theta}\right)_{ss} < 0$. Recalling that $\frac{d\Delta\theta}{dt} = i\omega\Delta\theta$, since a sinusoidal perturbation in ϕ always leads to a sinusoidal response in all variables, one can write for the faradaic admittance

$$Y_{far} = \frac{1}{R_{ct}} + \frac{m \, g_\phi}{i\omega - g_\theta}. \tag{3.6}$$

The total admittance of the electrochemical systems, finally, follows as

$$Y = Y_{far} + i\omega \, C_{dl} \tag{3.7}$$

where C_{dl} denotes the double layer capacity. The impedance is $Z(\omega) = \frac{1}{Y} = Z_{re} - i \, Z_{img}$. The Nyquist impedance plots shown in chapter 8 are obtained when plotting the Z_{img} versus Z_{re}. The notion of impedance can be rationalized as a quantity which relates the periodic input of a dynamical systems to its output (response) and therefore is equivalent to a linear open-loop transfer function in the engineering terminology.

Stability assessment and classification of electrochemical oscillators using impedance methods

The preceding section introduced impedance spectroscopy as a method to look for the linear response of a systems to a sinusoidal perturbation. If the periodic responses, expressed by Z_{re} and Z_{img}, are known over a wide frequency range, it is possible to make statements about the system's stability. The link between stability and impedance spectrum is the Nyquist stability criterion [46]. In its most rigorous form, the criterion is far from being straight-forward to use, so Koper suggested a simpler test which is entirely equivalent and allows the predictions of (local) bifurcations from an impedance spectrum [74, 23].

Linear stability analysis tells us that an externally driven system at a bifurcation encounters a condition of resonance where the driving signal is blown up by the system without delay. Hence, a bifurcation is a situation for which the impedance spectrum intersects the origin of the complex impedance plane. If the intersection occurs for non-zero frequency, the system exhibits a Hopf bifurcation; if the impedance spectrum terminates in the origin for zero frequency, the system exhibits a saddle-

node bifurcation. Clearly, as indicated above, the steady-state must be stable in order to measure the impedance properly. However, since the influence of an external ohmic resistance on the impedance spectrum amounts to a simple horizontal shift in the complex plane, it is easy to test graphically for the possibility of a Hopf or a saddle-node bifurcation from the impedance spectrum measured potentiostatically in the absence of an appreciable external ohmic resistance. Similar arguments hold for galvanostatic conditions. Koper [74] summarized the conditions for detecting bifurcations from impedance studies as follows.

For fixed applied potential (potentiostatic conditions), an electrochemical cell will exhibit

- a saddle-node bifurcation if $Z(\omega) = 0, \omega = 0$
- a Hopf bifurcation if $Z(\omega) = 0, \omega \neq 0$.

For fixed applied current (galvanostatic conditions), an electrochemical cell will exhibit

- a saddle-node bifurcation if $Y(\omega) = 0, \omega = 0$
- a Hopf bifurcation if $Y(\omega) = 0, \omega \neq 0$.

Recalling the mechanistic classification addressed in the previous chapter, one can now also relate the impedance spectra with the respective oscillator category NDR or HNDR. If the situation $Y(\omega) = 0, \omega \neq 0$ occurs under galvanostatic conditions or, equivalently, if a hidden negative impedance occurs, i.e. when $Z_{re} < 0$ at $\omega \neq 0$, but $Z_{re} \rightarrow 0$ for $\omega = 0$, then the oscillator considered belong to the HNDR class. If there is no hidden negative impedance and the impedance spectrum resembles Fig. 2a in ref. [74], the oscillator is uniquely identified as NDR oscillator. Chapter 9 will show, however, that this experimental identification on the basis of impedance spectroscopy is not unique in general, but involves certain assumption about the mechanism of the electrochemical oscillator under investigation.

Experimental measurements

Experimental impedance diagrams were obtained using a EG&G potentiostat (PAR 273A, Princeton Applied Research, Princeton) hooked up with a frequency response analyzer (S-5720, EC Electronic Instruments, Yokohama). The software installed allowed for a convenient control of the impedance parameters. Impedance data were saved on a IBM 486 personal computer.

3.2.4 Potential microprobe measurements

General remarks

Potential microprobes have been a classical tool in electrochemistry for monitoring local electrical potentials in electrolyte solutions. In experiments where the imaging

of spatiotemporal evolution of a potential distribution is of interest two or more local probes located along the electrified interface have frequently been employed.

As early as 1951 [13] Franck studied activation fronts in one space dimension with three stationary probes, whereas 15 electrode probes along Ni wires were involved in spatiotemporal potential measurements by Lev et al. [34]. Flätgen achieved one-dimensional imaging in an elegant rotating ring electrode setup with only one stationary potential microprobe near the rotating electrified surface [35, 84, 85, 86, 36]. He opted to use a rotating working electrode since the electrochemical reaction system used necessitated sufficient mass transport. By rotating a continuous scanning of the entire electrode is furthermore assured. Drawbacks of the rotating setup arise as soon as the rotation fails to be perfectly smooth and in-plane. Then, periodic potential artefacts arise in the microprobe signal which disturb the measurement.

Two-dimensional imaging with potential microprobes has been a challenging task and, therefore, has only been achieved in few systems such as metal corrosion [92, 93].

Two basic types of potential microprobes were described in the literature. One type is based on potentiometric probing and consists of a reference electrode, e.g. Hg/Hg_2SO_4 or $Ag/AgCl$, mounted in a glass tube which terminates in a small capillary (0.1 - 1000 μm in diameter). The glass tube is filled with an electrolyte solution. The other type involves a thin metal wire, e.g. Pt, which is sealed into a glass tube except for the tip which serves as the actual probe. While the former potential microprobes were usually used for the measurement of potential distributions with negligible current flowing through the capillary [93, 94, 95, 36], the latter were shown to readily provide information on mass transport, diffusion coefficients and interfacial kinetics [96, 97]. Furthermore, upon scanning along an electrochemical surface using a metal wire probe, an indirect imaging of the surface morphology becomes possible through feedback effects [97].

The present work opted for stationary potentiometric capillary probes for the study of spatiotemporal evolution of the potential inside the electrolyte near the working electrode. First, the general electrode setup of the measurements with two and eleven local potential probes will be described. Subsequently, the data acquisition setup used in chapter 6 will be discussed. Details concerning the electrode numbering and the solutions concentrations used will be given in the experimental section of chapter 6.

Two-potential-probe measurements

For the purpose of preliminary tests for spatial effects in an electrocatalytic system, a simple setup shown in Fig. 3-6 was designed. In contrast to previous studies in electrocatalytic systems [36] all parts, i.e. both working electrode and local potential probes, were stationary. A polycrystalline Pt ring electrode of 32,5 mm and 42,5 mm in inner and outer diameter was used as working electrode. The ring was pressed from Pt plate of 0.1 mm in thickness. The tip of a thin Pt wire - 0.3 mm in diameter and embedded in a 4mm glass tube except for the 3 mm tip - was welded onto the Pt plate ring at the a point near the outer edge to provide a connection of the Pt plate ring to the outer circuit. The glass tube was mounted into the teflon lid of the cell fixing the working electrode at a variable height within the electrolyte.

A polycrystalline Pt wire (1 mm in diameter) bended to a ring (62 mm in diameter) served as counter electrode and was placed concentrically to the working electrode (see Fig. 3-6). In analogy to the working electrode, a Pt wire inside a glass tube helped to fix the position of the counter electrode. Usually, throughout the spatial experiments, the counter electrode ring was placed about 50 mm above the working electrode ring plane.

The reference electrode (Hg/Hg_2SO_4) was mounted in a glass tube which terminated in a fine glass capillary (Luggin-Haber capillary) right in the center of the working electrode.

Two glass capillaries of approximately 200 μm inner diameter and 3mm length located at opposite sides of the upper face of the working electrode served as local potential probes. The upper end of the capillaries were attached to glass tubes of 8mm inner diameter which hosted the Hg/Hg_2SO_4 reference electrodes (Radiometer Corp.). The glass body of the local potential probe electrodes (8mm glass tube plus capillary) were filled with a highly concentrated electrolyte solution prior to air-free insertion of the reference electrodes. The complete local potential probes were thereafter mounted from above into the teflon cap of the cell. Subsequently, the lower, open end of the capillary was slowly approached towards the upper face of the working electrode up to a distance of approximately 300 - 1000 μm. In previous studies using local potentiometric probes [36] the capillaries were filled with Agar-Agar gel prepared with a highly-concentrated solution of some electrolyte. This treatment became necessary, since leakage of the electrolyte inside the local probes perturbed considerably the electrochemical process at the working electrode. In the present work, however, the use of gel for the reduction of diffusive leakage proved not to be critical, as identical electrolytes were used inside and outside the local probes and diffusive fluxes due to concentration drops did not qualitatively affect the spatiotemporal evolution of the potential near the working electrode.

Finally, an additional Pt-wire sealed in a glass tube except for a 2mm tip was mounted into the cell. This electrode served as 'pulse perturbation electrode' for the application of controlled spatially inhomogeneous perturbations of the potential distribution near the working electrode. Its Pt tip was approached to the upper face of the working electrode up to about 2mm.

Multi-potential-probe measurements

After preliminary tests on the capability of inhomogeneous spatiotemporal dynamical regimes in the chosen electrochemical reaction, the two-probe setup was extended and upscaled to eleven, identical equi-spaced local Hg/Hg_2SO_4 electrodes as illustrated in Fig. 3-7 in order to achieve an improved spatial resolution of the potential patterns. The general electrode and geometrical design was maintained. A modified teflon lid allowed the accommodation of eleven local probed along the working electrode in a 30 degree angle from each other. The design of each local probe was identical to that used in the two-probe measurements. Between the first and the eleventh potential probe, there remained a 60 degree gap where the pulse perturbation electrode was located. The working electrode and counter electrode during the multi-probe measurements

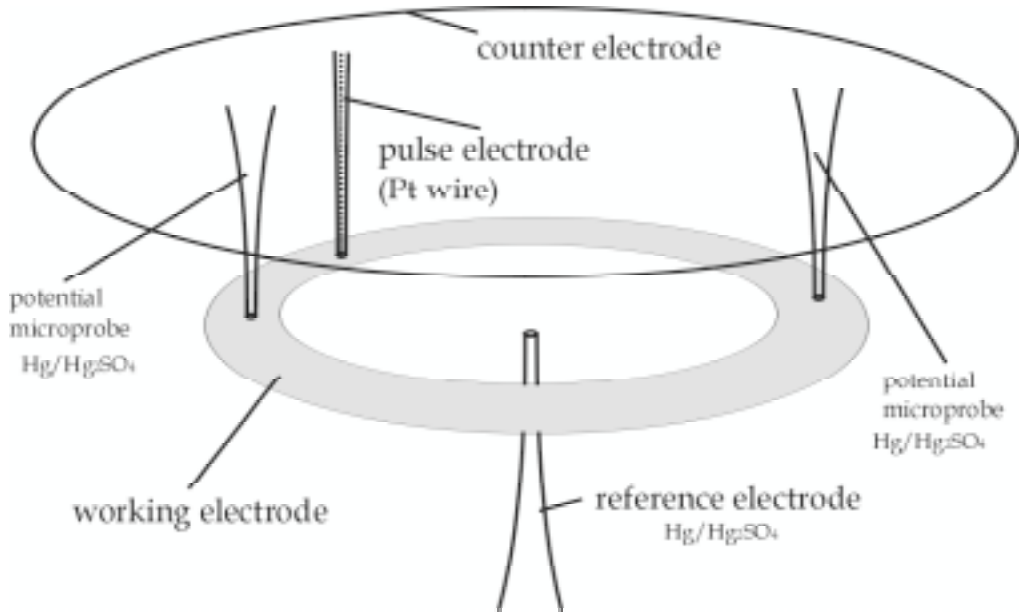

Figure 3-6: Experimental setup of the potentiometric two-probe local-potential measurements on a Pt-poly ring electrode.

were identical to those used in the two-probe studies. The reference electrode could now be shifted continuously along the axis of rotation of the working electrode.

Spatiotemporal resolution

The temporal resolution of the multi-probe setup is either given by the characteristic time scale τ of the potential probes, i.e. the time it takes for the probes to follow an abrupt change in potential near the working electrode or else by the reciprocal value of the sampling frequency f_{sample} of the A/D converter (see upcoming paragraph). The value of f_{sample} is given by the hard- and software configuration of the data acquisition setup. In order to minimize τ, the conductivity σ of the solution inside the capillary has to be maximized [36], for the capillary constitutes an electrical parallel RC circuit composed of the capillary's capacity and its solution resistance. For a typical value of the capillary capacity ($10^{-8}F$) and $\sigma$of the solutions employed, τ can be estimated to range from 0.1-10 μs which proved to be sufficient for the temporal processes considered.

The spatial resolution follows primarily from the spacing of the local probes along the electrode. Furthermore, the measured local potential value depends also on the individual distance of the probe from the electrode surface, since the distance determines the width of the spatial region over which an averaging of the potential occurs.

Generally, due to strong migration coupling the expected characteristic spatial

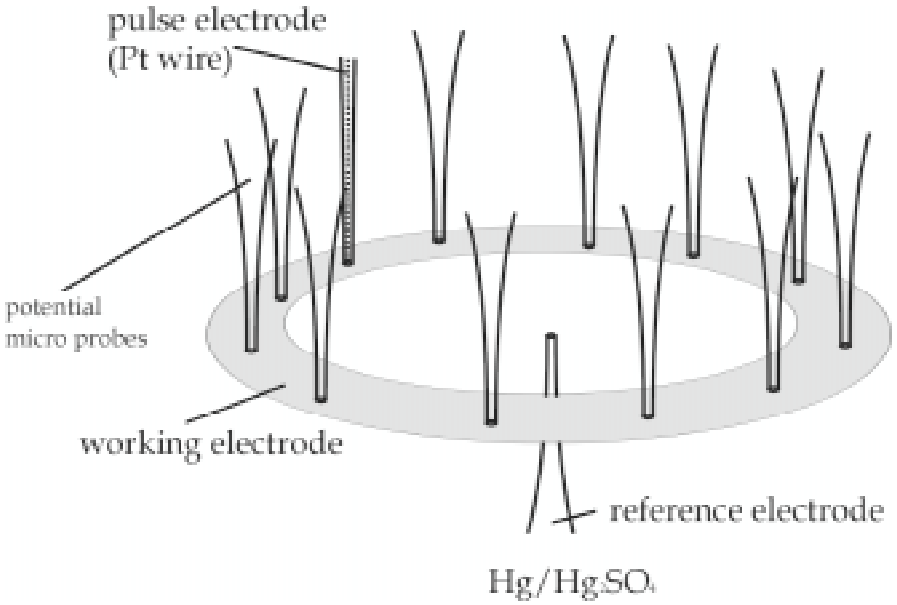

Figure 3-7: Side view of the multi-electrode array setup for the measurements of spatial potential distribution along a ring working electrode (counter electrode not shown).

length scale of electrochemical patterns is large compared to reaction-diffusion systems (RDS) and ranges well in the order of several mm (compared to 10 μm for surface RDS [27]). Therefore, the given basic spatial resolution of about 10 mm was assumed to be sufficient for the observation of spatial potential inhomogeneities.

The data acquisition setup

Fig. 3-8 sketches the principal elements involved in the complete experimental cell and data acquisition setup. The pulse perturbation electrode is connected to a pulse generator providing rectangular potential pulses of various duration and amplitude. Without external resistance, the amplitudes of the potential pulses are relative to the working electrode potential. Working, counter and reference electrodes are connected to the potentiostat/galvanostat which also controls an X-Y plotter. The local potential probes are connected through a combined low-pass filter/floating-ground amplifier (x10) (circuit is shown in Fig. 3-9) to the input channels of a 12 bit - 16 channel multiplex A/D converter. During measurements, the digital information is stored temporarily in the data acquisition device before it is passed on to a permanent storage (Personal Computer, Dell, Pentium 200 MHz) after completion of measurement.

The JAVA measurement software (written by H. Junkes and S. Schöne, Computational Center of the Fritz-Haber-Institut) is executed from the PC by clicking on START/Programme/Java Messprogramm/Peter's measurements. After window

pop-up, the software needs to be connected to the acquisition device (CPU with DNS entry 'link') by pressing 'connect'. The software is now by default set in the on-line, stand-by mode, i.e. a mode without storing information, but instead where the instantaneous potential information can be inspected in a time-series and a (potential-channel) plot representation. Upon starting the acquisition mode (START button), the instantaneous graphs are deactivated. Instead, the 16-channel information is read into the temporary memory and is transferred to the PC's hard disc after termination (STOP button). Apart from a setup information ASCII file including the information provided by the user in the lower window, an ASCII text file is created with 16 columns and the number of rows equalling the number of multiplexed input cycles. Being ASCII, the information is easily retrievable. The scanning frequency can continuously be varied between 10 and 1000 Hz.

System errors and data processing

With the A/D multiplex converter being 12 bit in resolution within a voltage range of $\pm$10 V, a maximal signal resolution of about 5 mV could be achieved in the local potential measurements.

This potential resolution was considered to be well sufficient, as potential variations due to dynamical instabilities were expected to be on the order of several hundred mV [98].

Apart from inherent measurement noise, systematic errors occurred due to variations (i) in the inner diameter of the eleven local capillary potential probes, (ii) in the ohmic potential drop across the electrolyte due to (α) spatially inhomogeneities of the conductivity of the electrolyte (leakage of the capillary solution) and (β) varying distance between the tip of the capillary and the working electrode surface.

While the variations of the innner diameter mainly affected the characteristic time scale of the capillaries and, therefore, did not considerably influence the magnitude of the measured local potential, variations of the solution conductivity inflicted the measured local potential, in particular at high ($\geq$ +0.5 V) and very low ($\leq$ -0.5V) overpotentials. At potentials considered under bistable and oscillatory conditions (around 0 V / Hg_2SO_4) the maximal system error of individual potential probes observed in experiments never exceeded 10 % (with respect to the average of the remaining ten electrode).

Since all local potential probes are stationary, data processing is straight-forward. Where a systematic error occurred, a linear renormalization was performed which allowed for the elimination of the systematic potential error. The only figure where this procedure was applied to one local probe is Fig. 6-12 in chapter 6.All potential/time and current/time plots in chapter 6 were obtained using Origin 5.0. All figures reproduce the original measurement data without any subsequent digital filtering.

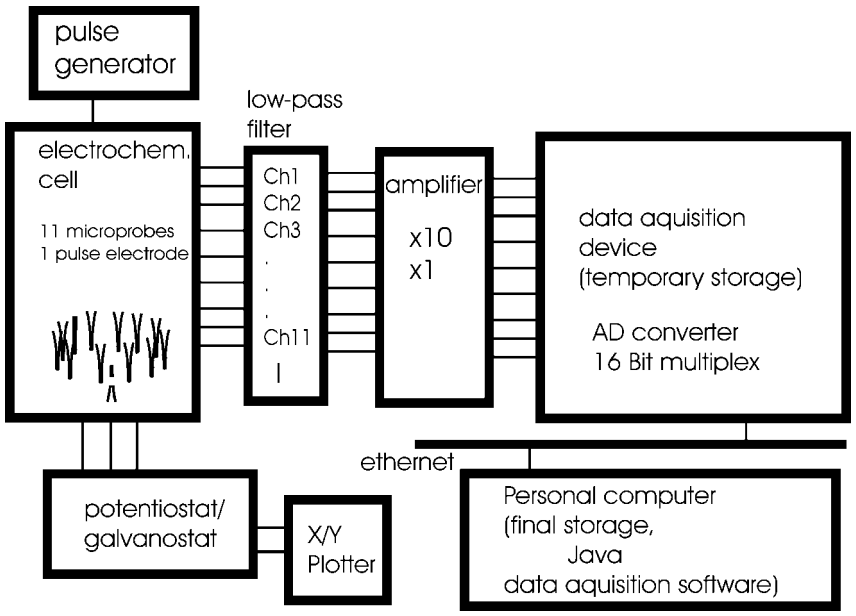

Figure 3-8: Principal experimental setup for data acquistion during multi-potential-probe measurements.

3.3 Theoretical concepts and methods

3.3.1 Essentials of process control

Complete control over the temporal and (for spatially extended systems) spatial dynamics of chemical reaction processes has always been a fundamental desire of chemists and chemical engineers alike. Chemical processes have been traditionally controlled by using linear systems analysis and design tools. These methods date back to the classical engineering control literature of the 1950's [99]. A major reason that the use of linear systems theory has been so pervasive is that there is an analytical solution, hence there are more rigorous stability and performance proofs. Also, the computational demands for linear system simulation (and implementation) are usually quite small when compared to a nonlinear simulation.

Obviously, the use of linear system technique is quite limiting if a chemical process is highly nonlinear. Therefore, ever since the advent of modern nonlinear systems theory [42], advanced nonlinear control strategies have been more and more put forward which are based on suggestions stemming from the field of theoretical physics and mathematics rather than from engineers. Unlike linear control techniques, nonlinear control strategies emphasize the exploitation of specific nonlinear feature in controlling a system's dynamics. Thus, nonlinear controllers are often specifically tailored to certain processes and cannot be easily adopted in different systems.[100, 101, 102].

Still, recent work also showed that in numerous cases conventional control solutions are able to control nonlinear behavior such as deterministic chaos [103, 104,

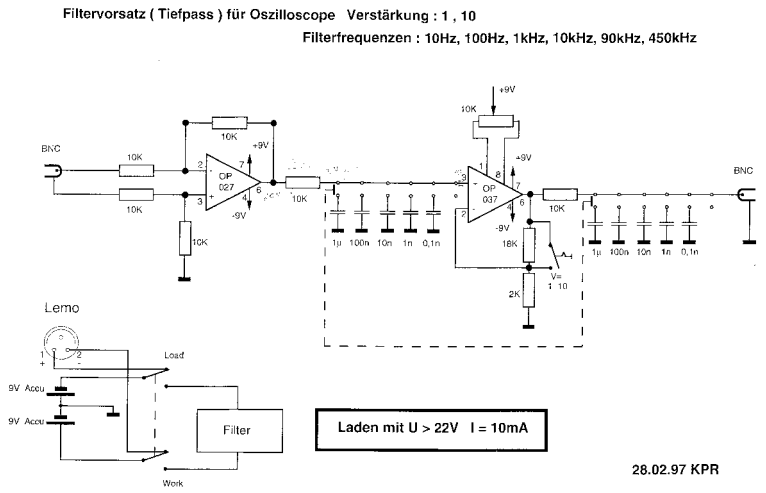

Figure 3-9: Electronic circuit of the amplifier and filter with floating ground used for the spatially resolved measurement of the local potential drop at the electrode surface.

105, 106]. This approach is important in that it not only offers a control engineering perspective to the control of complex systems but may also have laid some ground work for a more systematic and comprehensive study of the subject.

Notion and terminology of process control

A (chemical) process (control system) is characterized by a number of output variables y_i and one or more parameters accessible or unaccessible to the experimenter. The former are also referred to as constraints (M in Fig. 3-10). From an engineering point of view process control most generally denotes the action to make the process dynamics, i.e. the temporal evolution of one or more of the state variables to be controlled, follow a desired or prescribed path. Usually in engineering, it is implied that the process itself without any control action is in a stable stationary state, i.e. it is open-loop stable (see Fig. 3-10). Control action often follows from a discrepancy of the instantaneous value of the variables y_i to be controlled (control variable) and their setpoint value y^{SET}, i.e. their desired value. Control action is always exerted on system constraints. Feedback control measures the control variable, compares its value with its setpoint and feeds the error into a feedback controller which in turn manipulated a constraint. Information is thus fed back from the variables to a constraint (closed-loop control system). Action is taken after a change occurs in the process (see Fig. 3-11).

In the Nonlinear Dynamics's literature feedback process control usually deals with

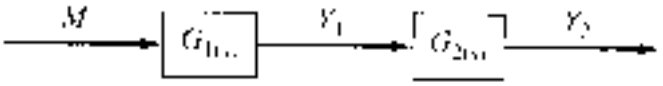

Figure 3-10: Scheme of an open-loop cascade control system. G_i represent the transfer functions of two consecutive processes in the Laplace domain.

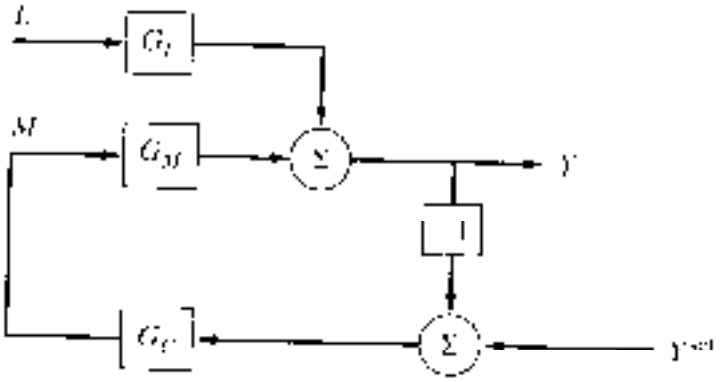

Figure 3-11: Scheme of a closed-loop control system. G_M,G_L,G_C denote the transfer functions of the process, the Load and the controller, respectively.

open-loop unstable systems (bistable, oscillatory or chaotic) with one or more unstable limit sets (repellors) coexisting with the stable attractor. Successful control involves the intensional change of stability of the limit sets without change of the value of the constraints or parameters. this type of control will be the subject of chapter 7 where an oscillatory open-loop system will be stabilized (controlled) onto the previously unstable and therefore unaccessible stationary state by means of conventional PID control techniques.

PID control

Proportional-Integral-Derivative (PID) control has been the dominant control strategy for decades and will remain the method used on a large fraction of all control problems for decades to come.

The PID algorithm in the time domain is

$$u(t) = k\left[e(t) + \frac{1}{\tau_I}\int_0^t e(t')\,dt' + \tau_D\frac{de(t)}{dt}\right] \tag{3.8}$$

$$e(t) = y^{SET} - y(t) \tag{3.9}$$

where u(t) denotes the manipulation of a constraint, k a proportional gain, τ_I and τ_D the integral and derivative time constant and e(t) the instantaneous error of the control variable.

More conveniently, controllers and control systems are described in the Laplace domain [107] using the Laplace variable s rather than in the time domain. In this representation, the control action on the eigenvalues (stability) of limit sets is much more transparent. An important concept in the Laplace domain is the ratio of the output and input values of process called the open-loop transfer function. Likewise, the transfer function of a controller can be defined in the Laplace domain. The transfer function completely determines the linear response of a system and is therefore related to the concept of impedance. In a closed-loop arrangement (Fig. 3-11), the overall feedback system can be described by a closed-loop transfer function which reads for the system in Fig. 3-11

$$G_{closed-loop} = \frac{y}{y^{SET}} = \frac{G_M G_C}{1 + G_M G_C}. \tag{3.10}$$

the roots of the denominator represent the eigenvalues of the complete system and thus determine the system stability.

Chemical process modeling

An important part of any control system design is the development of a mathematical representation of the process. Even if a linear control system design technique is used, verification is performed via simulations (see chapter 7).

Consider a nonlinear oscillatory model with state variable x and y and constraint p

$$\dot{x} = f(x, y, p) \tag{3.11}$$

$$\dot{y} = g(x, y) \tag{3.12}$$

Functions f and g are assumed to be sufficiently nonlinear for oscillations. Suppose there is an unstable stationary state (x_0, y_0) surrounded by a stable limit cycle at $p = p_0$, i.e. the system oscillates. The linearization of the system in the vicinity of the stationary steady state can be written as

$$\frac{d}{dt}\begin{pmatrix}\delta x\\ \delta y\end{pmatrix} = \begin{pmatrix} f_x & f_y\\ g_x & g_y\end{pmatrix}\begin{pmatrix}\delta x\\ \delta y\end{pmatrix} = J\begin{pmatrix}\delta x\\ \delta y\end{pmatrix} \tag{3.13}$$

with

$$Det\, J = f_x g_y - f_y g_x > 0 \tag{3.14}$$

$$Tr\, J = f_x + g_y > 0 \tag{3.15}$$

Upon feedback derivative control of y on p , the linear closed-loop system reads

$$\frac{d}{dt}\begin{pmatrix} \delta x \\ \delta y \end{pmatrix} = \begin{pmatrix} f_x & f_y \\ g_x & g_y \end{pmatrix}\begin{pmatrix} \delta x \\ \delta y \end{pmatrix} + B\, k\, \delta p \tag{3.16}$$

$$\delta p = \frac{d}{dt}\delta y = g_x\, \delta x + g_y\, \delta y \tag{3.17}$$

with k being the controller gain and $B = \binom{f_p}{g_p}$.

Hence, the overall closed-loop Jacobian yields

$$J' = \begin{pmatrix} f_x + f_p\, k\, g_x & f_y + f_p\, k\, g_y \\ g_x & g_y \end{pmatrix} \tag{3.18}$$

implying

$$Det\, J' = Det\, J > 0 \tag{3.19}$$

$$Tr\, J' = f_x + g_y + f_p\, k\, g_x \gtrless 0 \tag{3.20}$$

This means that by applying derivative control action only the trace of the linear system is altered and, thus, limit cycles can be selectively suppressed without altering the determinant given a negative value of the trace. Note that this simple additive control scheme holds only true as long as the control variable is not a function of the controlled constraint. In the latter case, an additional degree of freedom needs to be introduced in the system (see chapter 7).

3.3.2 Numerical methods

Integration. The numerical integration of systems of ordinary differential equations described in this thesis was performed using the FORTRAN lsode package [108]. This routine is a very reliable easy-to-use integration routine which is based on a higher-order Adams-Molten-type predictor-corrector method with automatic stepsize control. Absolute errors of the variables were fixed at 10^{-12}. The calculations were performed either on a DEC workstation (model 32000, Ultrix operating system, Digital corp.) or a Dec Alpha 400 (DEC OSF operating system).

Continuation. Continuation of local and global bifurcation points was performed with the non-interactive version of AUTO 86 written by Doedel [109]. This software traces out the saddle-node, Hopf, and saddle-loop bifurcation sets in two system parameters after an initial steady-state has been provided. In the upcoming two-parameter bifurcation diagrams Hopf and saddle-node bifurcations are always depicted as dashed and solid lines, respectively.